Furthermore, differentiating (35) w.r.t. various parameters gives

$$\frac{\partial \mathbf{R_w}}{\partial \Re\{c_1(i)\}} = \mathbf{T}_i \mathbf{R_z} \mathbb{C}_1^H + \mathbb{C}_1 \mathbf{T}_i^T \mathbf{R}_{bfz} \tag{45}$$

$$\frac{\partial \mathbf{R_w}}{\partial \Im\{c_1(i)\}} = j \cdot \left[\mathbf{T}_i \mathbf{R_z} \mathbb{C}_1^H - \mathbb{C}_1 \mathbf{T}_i^T \mathbf{R_z}\right] \tag{46}$$

$$\frac{\partial \mathbf{R_w}}{\partial \Re\{c_2(i)\}} = \mathbf{T}_i \mathbf{R_z} \mathbb{C}_2^H + \mathbb{C}_2 \mathbf{T}_i^T \mathbf{R_z} \tag{47}$$

$$\frac{\partial \mathbf{R_w}}{\partial \Im\{c_2(i)\}} = j \cdot \left[\mathbf{T}_i \mathbf{R_z} \mathbb{C}_2^H - \mathbb{C}_2 \mathbf{T}_i^T \mathbf{R_z}\right] \tag{48}$$

$$\partial \mathbf{R_w} \partial \varepsilon = \frac{\partial \mathbf{R_w}}{\partial \Re\{h(i)\}} = \frac{\partial \mathbf{R_w}}{\partial \Im\{h(i)\}} = \mathbf{0}_{N \times N}. \tag{49}$$

Substituting (37)–(39), (43), (44), and (45)–(49) back into (34) and inverting the resultant $\mathbf{J}$, we can obtain the CRB for $\boldsymbol{\eta}$. Therefore, we have $\mathrm{CRB}(\varepsilon) = [\mathbf{J}^{-1}]_{11}$.

REFERENCES

[1] C.-J. Hsu, R. Cheng, and W.-H. Sheen, "Joint least squares estimation of frequency, DC offset, I-Q imbalance, and channel in MIMO receivers," *IEEE Trans. Veh. Technol.*, vol. 58, no. 5, pp. 2201–2213, Jun. 2009.

[2] G.-T. Gil, I.-H. Sohn, J.-K. Park, and Y. H. Lee, "Joint ML estimation of carrier frequency, channel, I/Q mismatch, and DC offset in communication receivers," *IEEE Trans. Veh. Technol.*, vol. 54, no. 1, pp. 338–349, Jan. 2005.

[3] Y. H. Chung, K. D. Wu, and S. M. Phoong, "Joint estimation of I/Q imbalance, CFO and channel response for OFDM systems," in *Proc. IEEE ICASSP*, May 2009, pp. 2573–2576.

[4] J. Tubbax, B. Come, L. Van der Perre, S. Donnay, M. Engels, M. Moonen, and H. De Man, "Joint compensation of IQ imbalance and frequency offset in OFDM systems," in *Proc. Radio Wireless Conf.*, Boston, MA, Aug. 2003, pp. 39–42.

[5] S. Fouladifard and H. Shafiee, "Frequency offset estimation in OFDM systems in presence of IQ imbalance," in *Proc. IEEE ICC*, Anchorage, AK, May 2003, pp. 2071–2075.

[6] F. Yan, W.-P. Zhu, and M. O. Ahmad, "Carrier frequency offset estimation and I/Q imbalance compensation for OFDM systems," *EURASIP J. Adv. Signal Process.*, vol. 2007, pp. 1–11, 2007, Article ID 45364, DOI:10.1155/2007/45364.

[7] D. Tandur and M. Moonen, "Adaptive compensation of frequency-selective IQ imbalance and carrier frequency offset for OFDM based receivers," in *Proc. IEEE Workshop SPAWC*, Helsinki, Finland, Jun. 2007, pp. 1–5.

[8] H. Lin and K. Yamashita, "Subcarrier allocation based compensation for carrier frequency offset and I/Q imbalances in OFDM systems," *IEEE Trans. Wireless Commun.*, vol. 8, no. 1, pp. 18–23, Jan. 2009.

[9] G. Xing, M. Shen, and H. Liu, "Frequency offset and I/Q imbalance compensation for direct-conversion receivers," *IEEE Trans. Wireless Commun.*, vol. 4, no. 2, pp. 673–680, Mar. 2005.

[10] T. M. Schmidl and D. C. Cox, "Robust frequency and timing synchronization for OFDM," *IEEE Trans. Commun.*, vol. 45, no. 12, pp. 1613–1621, Dec. 1997.

[11] J. J. van de Beek, M. Sandell, and P. O. Borjesson, "ML estimation of time and frequency offset in OFDM systems," *IEEE Trans. Signal Process.*, vol. 45, no. 7, pp. 1800–1805, Jul. 1997.

[12] H. Minn, M. Zeng, and V. K. Bhargava, "On timing offset estimation for OFDM systems," *IEEE Commun. Lett.*, vol. 4, no. 7, pp. 242–244, Jul. 2000.

[13] K. Y. Sung and C. C. Chao, "Estimation and compensation of I/Q imbalance in OFDM direct-conversion receivers," *IEEE J. Sel. Topics Signal Process.*, vol. 3, no. 3, pp. 438–453, Jun. 2009.

[14] M. Valkama, M. Renfors, and V. Koivynen, "Compensation of frequency-selective I/Q imbalance in wideband receivers: Models and algorithms," in *Proc. IEEE SPAWC*, Mar. 2001, pp. 42–45.

[15] T. K. Moon and W. C. Stirling, *Mathematical Methods and Algorithms for Signal Processing*. Upper Saddle River, NJ: Prentice-Hall, 2000.

[16] S. M. Kay, *Fundamentals of Statistical Signal Processing*. Upper Saddle River, NJ: Prentice-Hall, 1998.

Channel Gain Map Tracking via Distributed Kriging

Emiliano Dall'Anese, *Member, IEEE*,
Seung-Jun Kim, *Member, IEEE*, and
Georgios B. Giannakis, *Fellow, IEEE*

***Abstract*—A collaborative algorithm is developed to estimate the channel gains of wireless links in a geographical area. The spatiotemporal evolution of shadow fading is characterized by judiciously extending an experimentally verified spatial-loss field model. Kriged Kalman filtering (KKF), which is a tool with widely appreciated merits in spatial statistics and geosciences, is adopted and implemented in a distributed fashion to track the time-varying shadowing field using a network of radiometers. The novel distributed KKF requires only local message passing yet achieves a global view of the radio frequency environment through consensus iterations. Numerical tests demonstrate superior tracking accuracy of the collaborative algorithm compared with its noncollaborative counterpart. Furthermore, the efficacy of the global channel gain knowledge obtained is showcased in the context of cognitive radio resource allocation.**

***Index Terms*—Channel tracking, cognitive radio, distributed algorithms, kriging, shadow fading.**

I. INTRODUCTION

Accurate characterization of the radio-frequency (RF) environment is critical for the design and analysis of wireless networks and for the adaptation of system parameters during operation. Conventionally, point-to-point feedback has been employed to acquire channel coefficients and interference levels on a per-link basis. Recently, because radios are endowed with more intelligence and cognition capabilities, significant departure from such a 1-D view of the RF environment has often been advocated [1].

Critical to this departure is the characterization of wireless fading links. The medium-scale fading or *shadowing* created by the attenuation and diffraction of propagating signals due to obstructions such as hills, buildings, and trees is particularly challenging to characterize, particularly when correlations among different locations and time instants are accounted for.

Well-established correlation models for shadow fading are available for cellular networks, in which mobile terminals are assumed to move with constant velocity [2]. Multihop relay scenarios were studied in [3]. An experimentally validated parametric model for nomadic and mobile distributed channels was reported in [4]. The importance of shadowing in analyzing the performance of wireless ad hoc networks was pointed out in [5], which introduced a model for capturing shadowing correlation between wireless links in the deployment area.

Manuscript received May 28, 2010; revised September 12, 2010, December 2, 2010, and January 12, 2011; accepted January 26, 2011. Date of publication February 10, 2011; date of current version March 21, 2011. This work was supported in part by the National Science Foundation under Grants CCF 0830480 and CON 0824007 and through a collaborative participation in the Communications and Networks Consortium sponsored by the U.S. Army Research Laboratory under the Collaborative Technology Alliance Program, Cooperative Agreement DAAD19-01-2-0011. The U.S. Government is authorized to reproduce and distribute reprints for Government purposes notwithstanding any copyright notation thereon. This paper was presented in part at the Second International Workshop on Cognitive Information Processing, Elba Island, Italy, June 2010. The review of this paper was coordinated by Dr. W. Zhuang.

The authors are with the Department of Electrical and Computer Engineering, University of Minnesota, 200 Union Street SE, Minneapolis, MN 55455 USA (e-mail: seungjun@umn.edu; emiliano@umn.edu; georgios@umn.edu).

Color versions of one or more of the figures in this paper are available online at http://ieeexplore.ieee.org.

Digital Object Identifier 10.1109/TVT.2011.2113195

Techniques for obtaining a spatial description of the RF environment are receiving growing interest. The ambient RF power spectrum was viewed as a random field in [6], and the Kriging technique was adopted to estimate the spatial power spectral density (PSD). Assuming that the PSD map is confined to a low-dimensional subspace, a distributed projection algorithm was devised in [7]. The PSD map was estimated by exploiting the underlying sparsity and a path-loss-based channel model in [8], whereas a spline interpolation technique was employed to accommodate shadow fading in [9].

This paper deals with tracking the spatiotemporal evolution of channel gains (CGs) in a given geographical area through a collaborative network of cognitive radios (CRs). Compared with the *local* CG maps, which predict the actual CGs from any point in space to the sensor locations [10], here, it is aimed to construct what is termed as a *global* CG map, which can, in addition, tell the CGs of wireless links that may completely be disjoint from the CR-to-CR links.

The CG maps are instrumental for the cross-layer design and assessment of the system-level performance of wireless networks [11], [12]. In CR networks, CG maps can provide vital information for spectrum sensing and resource allocation tasks [10], [13]. The latter application will explicitly be considered here to highlight the effectiveness of the CG maps.

To reconstruct the maps, the shadowing correlation model in [5] is judiciously extended to accommodate temporal variations. A distributed Kalman filtering (KF) scheme is then developed to track the mean field of shadow fading in space and time using messages that were exchanged among collaborating sensors. A *distributed* kriging interpolator is also developed to interpolate a spatially colored yet temporally white shadow-fading component. This paper is the first to model the spatiotemporal correlation of *any-to-any* CGs and develop the corresponding estimation algorithm in a distributed setup.

This paper is organized as follows. In Section II, a dynamic spatiotemporal shadow-fading model is introduced. The distributed kriged Kalman filtering (DKKF) algorithm is developed in Section III. In Section IV, the application of the global CG maps is discussed in the context of CR networks. Numerical results are presented in Section V followed by the conclusions in Section VI.

II. Dynamic Shadow-Fading Model

Consider a radio link from positions $\mathbf{x}$ to $\mathbf{y}$ at time t, where $\mathbf{x}$ and $\mathbf{y}$ are arbitrary points in a geographical area $\mathcal{A} \subset \mathbb{R}^2$. The link gain can be decomposed into path-loss, shadowing, and small-scale fading components [14]. By averaging out the effect of small-scale fading, the averaged CG function $G_{\mathbf{x}\to\mathbf{y}}(t)$ of link $\mathbf{x} \to \mathbf{y}$ at time t, which is expressed in decibels, can be written as

$$G_{\mathbf{x}\to\mathbf{y}}(t) = G_0 - 10\gamma \log_{10}(\|\mathbf{x}-\mathbf{y}\|) + s_{\mathbf{x}\to\mathbf{y}}(t) \tag{1}$$

where $\|\cdot\|$ is the Euclidean norm, G_0 is the path gain at the unit distance, γ is the path-loss exponent, and $s_{\mathbf{x}\to\mathbf{y}}(t)$ is the shadow-fading component (in decibels), which is Gaussian distributed [14, p. 104].

One challenge in the statistical modeling of shadowing lies in characterizing its spatiotemporal correlation. In an effort to establish a shadowing correlation model that is suitable to ad hoc network scenarios, the concept of *spatial-loss field* was introduced in [5]. The spatial-loss field essentially captures the obstructions in the area where the network is deployed. The shadowing effects experienced by individual links in the network are then modeled by line integrals of this common field. The resulting shadow-fading correlation matches field measurements, as well as the conventional correlation models in the literature [5]. The scope of this approach is considerably broadened here by also incorporating the temporal dynamics. This approach allows us to employ the powerful machinery of KKF [15], [16] to track the spatiotemporal shadowing evolution online.

Let $\ell(\mathbf{x},t)$ denote the spatial-loss field at location $\mathbf{x} \in \mathcal{A}$ at time t, which is assumed to be Gaussian [5]. The spatiotemporal dynamics of the spatial-loss field are characterized by [16]

$$\begin{aligned} \ell(\mathbf{x},t) &= \bar{\ell}(\mathbf{x},t) + \tilde{\ell}(\mathbf{x},t) \text{ and} \\ \bar{\ell}(\mathbf{x},t) &= \int_{\mathcal{A}} w(\mathbf{x},\mathbf{u})\bar{\ell}(\mathbf{u},t-1)\,d\mathbf{u} + \eta(\mathbf{x},t) \end{aligned} \tag{2}$$

where $\bar{\ell}(\mathbf{x},t)$ represents the component that is colored in both space and time through the filter $w(\mathbf{x},\mathbf{u})$ that captures the interaction of loss $\bar{\ell}$ at position $\mathbf{x}$ at time t, with the loss $\bar{\ell}$ at position $\mathbf{u}$ at time $t-1$, $\tilde{\ell}(\mathbf{x},t)$ and $\eta(\mathbf{x},t)$ are spatially colored yet temporally white zero-mean Gaussian stationary random fields. Process $\eta(\mathbf{x},t)$ captures unmodeled dynamics that are uncorrelated with $\tilde{\ell}(\mathbf{u},\tau)$, $\forall \mathbf{u},\tau$. Moreover, $\mathbb{E}\{\tilde{\ell}(\mathbf{x},t)\bar{\ell}(\mathbf{u},t)\} = \mathbb{E}\{\eta(\mathbf{x},t)\bar{\ell}(\mathbf{u},t-1)\} = 0$ for all $\mathbf{x}$, $\mathbf{u}$, and t. For stability, the filter $w(\mathbf{x},\mathbf{u})$ must satisfy $|\int_{\mathcal{A}} w(\mathbf{x},\mathbf{u})d\mathbf{u}| < 1$, $\forall \mathbf{x}$.

The state-space model described by (2) is infinite-dimensional. One standard approach for reducing its dimensionality and computationally rendering it tractable from a signal processing perspective is to employ a basis-expansion representation [10], [16], [17]. In particular, introduce a complete orthonormal basis $\{\psi_k(\cdot)\}_{k=1}^{\infty}$ defined on $\mathcal{A}$ such that $\bar{\ell}(\mathbf{x},t) = \sum_{k=1}^{\infty} \alpha_k(t)\psi_k(\mathbf{x})$ and $w(\mathbf{x},\mathbf{u}) = \sum_{k=1}^{\infty} \beta_k(\mathbf{x})\psi_k(\mathbf{u})$. Then, similar to [10], only the K dominant terms are retained in the expansions, and N_r sampling (measurement) positions $\{\mathbf{x}_r \in \mathcal{A}\}_{r=1}^{N_r}$ are considered. Letting $\mathbf{\Psi}$ and $\mathbf{B}$ denote $(N_r \times K)$-matrices that collect coefficients $\{\psi_k(\mathbf{x}_r)\}$ and $\{\beta_k(\mathbf{x}_r)\}$, respectively, and defining $\boldsymbol{\alpha}(t) \triangleq [\alpha_1(t),\ldots,\alpha_K(t)]^T$, we obtain the state evolution equation

$$\boldsymbol{\alpha}(t) = \mathbf{T}\boldsymbol{\alpha}(t-1) + \mathbf{\Psi}^{\dagger}\boldsymbol{\eta}(t) \tag{3}$$

where $\boldsymbol{\eta}(t) \triangleq [\eta(\mathbf{x}_1,t) \quad \ldots \quad \eta(\mathbf{x}_{N_r},t)]^T$, $\mathbf{\Psi}^{\dagger} \triangleq (\mathbf{\Psi}^T\mathbf{\Psi})^{-1}\mathbf{\Psi}^T$, and $\mathbf{T} \triangleq \mathbf{\Psi}^{\dagger}\mathbf{B}$.

Using the loss function ℓ, the shadowing (in decibels) for the link $\mathbf{x} \to \mathbf{y}$ is modeled as [5]

$$s_{\mathbf{x}\to\mathbf{y}}(t) = \frac{1}{\|\mathbf{x}-\mathbf{y}\|^{\frac{1}{2}}} \int_{\mathbf{x}\to\mathbf{y}} \ell(\mathbf{u},t)\,d\mathbf{u} \tag{4}$$

which yields $s_{\mathbf{x}\to\mathbf{y}}(t) = \bar{s}_{\mathbf{x}\to\mathbf{y}}(t) + \tilde{s}_{\mathbf{x}\to\mathbf{y}}(t)$, with $\bar{s}_{\mathbf{x}\to\mathbf{y}}$ and $\tilde{s}_{\mathbf{x}\to\mathbf{y}}$ defined in the obvious manner; cf. (2). In particular, $\bar{s}_{\mathbf{x}\to\mathbf{y}}(t)$ can be approximated as

$$\bar{s}_{\mathbf{x}\to\mathbf{y}}(t) = \sum_{k=1}^{\infty} \underbrace{\left[\frac{1}{\|\mathbf{x}-\mathbf{y}\|^{1/2}} \int_{\mathbf{x}\to\mathbf{y}} \psi_k(\mathbf{u})d\mathbf{u}\right]}_{\triangleq \phi_{\mathbf{x}\to\mathbf{y},k}} \alpha_k(t) \approx \boldsymbol{\phi}_{\mathbf{x}\to\mathbf{y}}^T\boldsymbol{\alpha}(t) \tag{5}$$

where $\boldsymbol{\phi}_{\mathbf{x}\to\mathbf{y}} \triangleq [\phi_{\mathbf{x}\to\mathbf{y},1} \quad \ldots \quad \phi_{\mathbf{x}\to\mathbf{y},K}]^T$ depends only on the spatial coordinates $\mathbf{x}$ and $\mathbf{y}$.

Next, the spatial correlation model for $\tilde{s}_{\mathbf{x}\to\mathbf{y}}(t)$ is established. To this end, the spatial correlation of $\tilde{\ell}(\mathbf{x},t)$ needs to first be modeled. Given $\boldsymbol{\alpha}(t)$, $\bar{s}_{\mathbf{x}\to\mathbf{x}_r}(t)$ represents the deterministic time-varying mean of the shadowing $s_{\mathbf{x}\to\mathbf{x}_r}(t)$, which is referred to as a *trend* in spatial statistics [18]. Likewise, conditioned on $\boldsymbol{\alpha}(t)$, $\bar{\ell}(\mathbf{x},t)$ corresponds to the trend of the spatial-loss field $\ell(\mathbf{x},t)$. Noting that [5] models spatial-loss effects as a zero-mean random field reveals that the modeling and analysis in [5] hold for the *detrended* zero-mean random field $\tilde{\ell}(\mathbf{x},t)$ in the present context. This condition justifies modeling $\tilde{\ell}(\mathbf{x},t)$ to have

exponentially decaying correlation the same way that [5] modeled the spatial-loss field; see [10] for further justification. Then, the cross correlation $C_{\tilde{s}}(\mathbf{x}\to\mathbf{y},\mathbf{u}\to\mathbf{v}) \triangleq \mathbb{E}\{\tilde{s}_{\mathbf{x}\to\mathbf{y}}(t)\tilde{s}_{\mathbf{u}\to\mathbf{v}}(t)\}$ of $\tilde{s}_{\mathbf{x}\to\mathbf{y}}(t)$ and $\tilde{s}_{\mathbf{u}\to\mathbf{v}}(t)$ for arbitrary links $\mathbf{x}\to\mathbf{y}$ and $\mathbf{u}\to\mathbf{v}$ is given by [cf. (4)]

$$C_{\tilde{s}}(\mathbf{x}\to\mathbf{y},\mathbf{u}\to\mathbf{v}) = \frac{\sigma_{\tilde{s}}^2}{d_{\tilde{\ell}}\|\mathbf{x}-\mathbf{y}\|^{\frac{1}{2}}\|\mathbf{u}-\mathbf{v}\|^{\frac{1}{2}}} \cdot \int_{\mathbf{x}\to\mathbf{y}}\int_{\mathbf{u}\to\mathbf{v}} \exp\left(-\frac{\|\mathbf{x}_1-\mathbf{x}_2\|}{d_{\tilde{\ell}}}\right) d\mathbf{x}_1^T\, d\mathbf{x}_2 \quad (6)$$

where $\sigma_{\tilde{s}}^2$ is the variance of process $\tilde{s}_{\mathbf{x}\to\mathbf{y}}(t)$, and $d_{\tilde{\ell}}$ is the coherence distance of the $\tilde{\ell}$-field.

Under this cross-correlation model, a shadowing estimate of link $\mathbf{x}\to\mathbf{y}$ between *any* points $\mathbf{x}$ and $\mathbf{y}$ in $\mathcal{A}$ can be obtained by spatially interpolating and temporally filtering measurements $\{s_{\mathbf{x}_j\to\mathbf{x}_r}(t)\}_{j,r\in\{1,\ldots,N_r\},j\neq r}$ made for a set of links in $\mathcal{A}$, which may be disjoint from link $\mathbf{x}\to\mathbf{y}$.

III. Map Tracking via Distributed Kriged Kalman Filtering

Kriged Kalman filtering (KKF) is a universal kriging approach [18], where the spatiotemporal evolution of the trend field $\bar{s}$ is tracked through KF. Based on the model in Section II, it is clear that estimating the trend field $\bar{s}_{\mathbf{x}\to\mathbf{y}}(t)$ can benefit from fusing the observations of all sensors. This approach will be accomplished by a distributed KF algorithm, which does not require all the measurements to be collected at a fusion center. The shadow-fading map $s_{\mathbf{x}\to\mathbf{y}}(t)$ can then be tracked $\forall\,\mathbf{x},\mathbf{y},t$ by complementing the trend estimate with an estimate of $\tilde{s}_{\mathbf{x}\to\mathbf{y}}(t)$ obtained through distributed kriging. To this end, it is necessary to set up a measurement model.

Remark 1: A noncollaborative KKF approach, which does not involve the spatial-loss field model, was developed in [10]. However, compared with [10], the approach presented here introduces collaboration among sensors and, more importantly, allows the prediction of the CGs on wireless links that might be completely disjoint from the measured links. ■

A. Measurement Model

Consider a network of N_r CRs at positions known to one another, which exchange training signals to estimate the gains of their channels. Suppose that CR $j(\neq r)$ transmits a unit-power training signal for CR r to acquire an estimate of $G_{\mathbf{x}_j\to\mathbf{x}_r}(t)$ by simply measuring the received power. Using (1), it is then possible to obtain a noisy measurement of $s_{\mathbf{x}_j\to\mathbf{x}_r}(t)$ modeled as $\breve{s}_{\mathbf{x}_j\to\mathbf{x}_r}(t) = s_{\mathbf{x}_j\to\mathbf{x}_r}(t) + \epsilon_{\mathbf{x}_j\to\mathbf{x}_r}(t)$, where $\epsilon_{\mathbf{x}_j\to\mathbf{x}_r}(t)$ denotes zero-mean Gaussian measurement noise that results from averaging out small-scale fading and interference [10]. Suppose that each sensor r can measure the received powers from the transmissions of the set $\mathcal{M}_r$ of sensors, where $\mathcal{M}_r \subset \{1,\ldots,N_r\}\setminus\{r\}$. Let M_r be the cardinality of $\mathcal{M}_r$, and $M \triangleq \sum_{r=1}^{N_r} M_r$. Let $\breve{\mathbf{s}}_r(t)$ denote the M_r-vector that collects $\{\breve{s}_{\mathbf{x}_j\to\mathbf{x}_r}(t)\}$, $j\in\mathcal{M}_r$. Then, by pooling measurements from all sensors to an $(M\times 1)$-supervector $\breve{\mathbf{s}}(t) \triangleq [\breve{\mathbf{s}}_1^T(t) \quad \ldots \quad \breve{\mathbf{s}}_{N_r}^T(t)]^T$, we can write [cf. (5)]

$$\breve{\mathbf{s}}(t) = \boldsymbol{\Phi}\boldsymbol{\alpha}(t) + \tilde{\mathbf{s}}(t) + \boldsymbol{\epsilon}(t) \quad (7)$$

where $\boldsymbol{\Phi}$, $\tilde{\mathbf{s}}(t)$, and $\boldsymbol{\epsilon}(t)$ are constructed from $\{\boldsymbol{\phi}_{\mathbf{x}_j\to\mathbf{x}_r}^T\}$, $\{\tilde{s}_{\mathbf{x}_j\to\mathbf{x}_r}(t)\}$, and $\{\epsilon_{\mathbf{x}_j\to\mathbf{x}_r}(t)\}$, $j\in\mathcal{M}_r$, $r=1,\ldots,N_r$, respectively, in the obvious way.

B. Distributed Kriged Kalman Filtering

Given the state (3) and the measurement (7) equations, the minimum mean square error (MMSE) estimate of the state vector $\boldsymbol{\alpha}(t)$ at time t can be obtained through an ordinary KF. Define $\mathbf{C}_{\tilde{s}} \triangleq \mathrm{cov}\{\tilde{\mathbf{s}}(t)\}$, $\mathbf{C}_{\epsilon} \triangleq \mathrm{cov}\{\boldsymbol{\epsilon}(t)\}$, $\mathbf{C}_{\eta} \triangleq \mathrm{cov}\{\boldsymbol{\eta}(t)\}$, and $\boldsymbol{\Sigma} \triangleq \mathbf{C}_{\tilde{s}} + \mathbf{C}_{\epsilon}$. In addition, let $\breve{\mathbf{S}}(t)$ denote the $(M\times t)$-matrix that contains the cumulative measurements $\{\breve{\mathbf{s}}(\tau)\}_{\tau=1}^t$.

Upon defining $\hat{\boldsymbol{\alpha}}(t|t-1) \triangleq \mathbb{E}\{\boldsymbol{\alpha}(t)|\breve{\mathbf{S}}(t-1)\}$, $\hat{\boldsymbol{\alpha}}(t|t) \triangleq \mathbb{E}\{\boldsymbol{\alpha}(t)|\breve{\mathbf{S}}(t)\}$, $\mathbf{P}(t|t-1) \triangleq \mathrm{cov}\{\boldsymbol{\alpha}(t)|\breve{\mathbf{S}}(t-1)\}$, and $\mathbf{P}(t|t) \triangleq \mathrm{cov}\{\boldsymbol{\alpha}(t)|\breve{\mathbf{S}}(t)\}$, the KF equations in the information form are

$$\mathbf{P}(t|t-1) = \mathbf{T}\mathbf{P}(t-1|t-1)\mathbf{T}^T + \boldsymbol{\Psi}^{\dagger}\mathbf{C}_{\eta}\boldsymbol{\Psi}^{\dagger\,T} \quad (8)$$

$$\hat{\boldsymbol{\alpha}}(t|t-1) = \mathbf{T}\hat{\boldsymbol{\alpha}}(t-1|t-1) \quad (9)$$

$$\mathbf{P}(t|t) = \left[\boldsymbol{\Phi}^T\boldsymbol{\Sigma}^{-1}\boldsymbol{\Phi} + \mathbf{P}^{-1}(t|t-1)\right]^{-1} \quad (10)$$

$$\hat{\boldsymbol{\alpha}}(t|t) = \hat{\boldsymbol{\alpha}}(t|t-1) + \mathbf{P}(t|t)\boldsymbol{\Phi}^T\boldsymbol{\Sigma}^{-1}\left[\breve{\mathbf{s}}(t) - \boldsymbol{\Phi}\hat{\boldsymbol{\alpha}}(t|t-1)\right]. \quad (11)$$

Note that the line integral that transforms the spatial-loss field to shadow fading has been absorbed into $\boldsymbol{\phi}_{\mathbf{x}\to\mathbf{y}}$ for the "trend" part through (5) and the cross-correlation structure for $\tilde{s}_{\mathbf{x}\to\mathbf{y}}$ is directly modeled through (6). Therefore, the model well fits into the KKF framework delineated in [10] and [17]. That is, because the peculiarities of adopting the spatial-loss field model have completely been absorbed by the state space model, and the measurements are jointly Gaussian with the shadowing field, the proposition in [10] and [17], which was adopted here for the collective measurements, applies. It reveals that the KF-based trend estimate augmented by kriging spatial interpolation yields the desired MMSE estimate of the shadowing field.

Proposition 1: Conditioned on the measurements $\breve{\mathbf{S}}(t)$, the shadow fading $s_{\mathbf{x}\to\mathbf{y}}(t)$ for any $\mathbf{x},\mathbf{y}\in\mathcal{A}$, is Gaussian distributed with the mean and variance given, respectively, by

$$\begin{aligned}\hat{s}_{\mathbf{x}\to\mathbf{y}}(t) &\triangleq \mathbb{E}\left\{s_{\mathbf{x}\to\mathbf{y}}(t)|\breve{\mathbf{S}}(t)\right\} \\ &= \boldsymbol{\phi}_{\mathbf{x}\to\mathbf{y}}^T\hat{\boldsymbol{\alpha}}(t|t) \\ &\quad + \mathbf{c}_{\tilde{s}}^T(\mathbf{x},\mathbf{y})\boldsymbol{\Sigma}^{-1}\left[\breve{\mathbf{s}}(t) - \boldsymbol{\Phi}\hat{\boldsymbol{\alpha}}(t|t)\right] \quad (12)\end{aligned}$$

$$\begin{aligned}\mathrm{var}\left\{s_{\mathbf{x}\to\mathbf{y}}(t)|\breve{\mathbf{S}}(t)\right\} &= \sigma_{\tilde{s}}^2 - \mathbf{c}_{\tilde{s}}^T(\mathbf{x},\mathbf{y})\boldsymbol{\Sigma}^{-1}\mathbf{c}_{\tilde{s}}(\mathbf{x},\mathbf{y}) \\ &\quad + \left[\boldsymbol{\phi}_{\mathbf{x}\to\mathbf{y}}^T - \mathbf{c}_{\tilde{s}}^T(\mathbf{x},\mathbf{y})\boldsymbol{\Sigma}^{-1}\boldsymbol{\Phi}\right]\mathbf{P}(t|t) \\ &\quad \cdot \left[\boldsymbol{\phi}_{\mathbf{x}\to\mathbf{y}} - \boldsymbol{\Phi}^T\boldsymbol{\Sigma}^{-1}\mathbf{c}_{\tilde{s}}(\mathbf{x},\mathbf{y})\right] \quad (13)\end{aligned}$$

where $\mathbf{c}_{\tilde{s}}(\mathbf{x},\mathbf{y}) \triangleq \mathbb{E}\{\tilde{\mathbf{s}}(t)\tilde{s}_{\mathbf{x}\to\mathbf{y}}(t)\}$.

Remark 2: The model covariances $\mathbf{C}_{\epsilon}$, $\mathbf{C}_{\eta}$ and $\mathbf{C}_{\tilde{s}}$, as well as the state transition matrix $\mathbf{T}$, can be estimated similar to [10]. To estimate $\sigma_{\tilde{s}}^2$ and $d_{\tilde{\ell}}$ in (6), an exhaustive search over the $(\sigma_{\tilde{s}}^2, d_{\tilde{\ell}})$-space is performed. In particular, with $\hat{\mathbf{C}}_{\tilde{s}}$ denoting the sample covariance estimate of $\tilde{\mathbf{s}}(t)$ based on the procedure described in [10], the parameters $(\sigma_{\tilde{s}}^2, d_{\tilde{\ell}})$ that minimize the cost $\|\hat{\mathbf{C}}_{\tilde{s}} - \mathbf{C}_{\tilde{s}}(\sigma_{\tilde{s}}^2, d_{\tilde{\ell}})\|_F^2$ are found, where $\mathbf{C}_{\tilde{s}}(\sigma_{\tilde{s}}^2, d_{\tilde{\ell}})$ is computed through the model (6). ■

Given that matrices $\mathbf{T}$, $\boldsymbol{\Sigma}$, and $\boldsymbol{\Psi}^{\dagger}\mathbf{C}_{\eta}\boldsymbol{\Psi}^{\dagger\,T}$ are known to all sensors, the prediction step in (8) and (9) can locally be performed at each node, provided that $\hat{\boldsymbol{\alpha}}(t-1|t-1)$ and $\mathbf{P}(t-1|t-1)$ are available. However, to perform the correction step in (11), the measurements from other sensors are required. To reduce the substantial message-passing overhead associated with globally sharing (i.e., flooding) the measurements in each update step, a distributed algorithm is desired. To this end, consider the innovation process $\mathbf{y}(t) \triangleq \breve{\mathbf{s}}(t) - \boldsymbol{\Phi}\hat{\boldsymbol{\alpha}}(t|t-1)$ and define a $(K\times 1)$-vector $\boldsymbol{\chi}(t) \triangleq \boldsymbol{\Phi}^T\boldsymbol{\Sigma}^{-1}\mathbf{y}(t)$. It is clear from (11) that, if $\boldsymbol{\chi}(t)$ was available at each sensor, the Kalman steps in (8)-(11) could locally be performed at individual sensors.

To distribute the computation of $\boldsymbol{\chi}(t)$, consider rewriting it as a sum of N_r terms, each of which contains only local information. Let

$\mathbf{H}_r$ denote the $(K \times M_r)$-matrix formed by the $(\sum_{r'=1}^{r-1} M_{r'}+1)$th to the $(\sum_{r'=1}^{r} M_{r'})$th columns of $\mathbf{\Phi}^T\mathbf{\Sigma}^{-1}$. Using $\mathbf{H}_r$ and $\mathbf{y}_r(t) \triangleq \breve{\mathbf{s}}_r(t) - \mathbf{\Phi}_r\boldsymbol{\alpha}(t|t-1)$, it is possible to express $\boldsymbol{\chi}(t)$ as $\boldsymbol{\chi}(t) = \sum_{r=1}^{N_r} \mathbf{H}_r\mathbf{y}_r(t)$, which is equivalent to

$$\boldsymbol{\chi}(t) = \arg\min_{\boldsymbol{\chi}} \sum_{r=1}^{N_r} \|\boldsymbol{\chi} - N_r\mathbf{H}_r\mathbf{y}_r(t)\|^2 . \tag{14}$$

To distribute (14), introduce local copies of $\boldsymbol{\chi}(t)$ per sensor and denote these copies as $\boldsymbol{\chi}_r(t)$, $r = 1, 2, \ldots, N_r$. Then, (14) can be reformulated as the following constrained optimization problem:

$$\{\boldsymbol{\chi}_r(t)\}_{r=1}^{N_r} = \arg\min_{\{\boldsymbol{\chi}_r\}} \sum_{r=1}^{N_r} \|\boldsymbol{\chi}_r - N_r\mathbf{H}_r\mathbf{y}_r(t)\|^2 \tag{15}$$

$$\text{subject to } \boldsymbol{\chi}_r = \boldsymbol{\chi}_\varrho \quad \forall\, \varrho \in \mathcal{N}_r \quad r = 1, \ldots, N_r \tag{16}$$

where the constraints in (16) enforce the local copies of $\boldsymbol{\chi}(t)$ to coincide within the set of one-hop neighbors $\mathcal{N}_r$ of node r, $\forall r \in \{1, 2, \ldots, N_r\}$. Assuming that the network remains connected, i.e., there exist (possibly multihop) paths from any node to any other node in the network, the constraints in (16) ensure global consensus on $\boldsymbol{\chi}_r(t), \forall\, r = 1, \ldots, N_r$.

Employing the alternating direction method of multipliers (ADMoM), we can show that the following iterative algorithm attains the solution to (15) and (16) (see also, e.g., [10]):

$$\boldsymbol{\zeta}_r^{(j)}(t) = \boldsymbol{\zeta}_r^{(j-1)}(t) + \kappa\left(|\mathcal{N}_r|\boldsymbol{\chi}_r^{(j)}(t) - \sum_{\varrho\in\mathcal{N}_r} \boldsymbol{\chi}_\varrho^{(j)}(t)\right) \tag{17}$$

$$\boldsymbol{\chi}_r^{(j+1)}(t) = (1+\kappa|\mathcal{N}_r|)^{-1} \times \left[N_r\mathbf{H}_r\mathbf{y}_r(t) - \frac{1}{2}\boldsymbol{\zeta}_r^{(j)}(t) + \frac{\kappa}{2} \times \left(|\mathcal{N}_r|\boldsymbol{\chi}_r^{(j)}(t) + \sum_{\varrho\in\mathcal{N}_r} \boldsymbol{\chi}_\varrho^{(j)}(t)\right)\right] \tag{18}$$

where $\boldsymbol{\zeta}_r^{(j)}(t)$ denotes the Lagrange multiplier that corresponds to (16) updated at sensor r during the KF iteration indexed by t, superscript j indexes consensus iterations, $\kappa > 0$ is a constant that can arbitrarily be chosen, and $|\mathcal{N}_r|$ denotes the cardinality of the set $\mathcal{N}_r$.

At iteration j, sensor r needs to collect from its neighbors the current estimates $\{\boldsymbol{\chi}_\varrho^{(j)}(t)\}_{\varrho\in\mathcal{N}_r}$ to update the auxiliary vector $\boldsymbol{\zeta}_r^{(j)}(t)$ through (17) and to subsequently compute $\boldsymbol{\chi}_r^{(j+1)}(t)$ through (18). The derivation of (17) and (18) and the proof of the convergence result are analogous to the derivation and proof in [10, App. C] and are omitted here for brevity.

To locally obtain $\hat{s}_{\mathbf{x}\to\mathbf{y}}(t)$ in (12) per CR, it is first noted based on (11) that

$$\mathbf{c}_{\breve{s}}^T(\mathbf{x},\mathbf{y})\mathbf{\Sigma}^{-1}\left[\breve{\mathbf{s}}(t) - \mathbf{\Phi}\hat{\boldsymbol{\alpha}}(t|t)\right] = \mathbf{c}_{\breve{s}}^T(\mathbf{x},\mathbf{y})\mathbf{\Sigma}^{-1}\mathbf{y}(t) - \mathbf{c}_{\breve{s}}^T(\mathbf{x},\mathbf{y})\mathbf{\Sigma}^{-1}\mathbf{\Phi}\mathbf{P}(t|t)\boldsymbol{\chi}(t). \tag{19}$$

Thus, we only need to distributively obtain $\xi(t) \triangleq \mathbf{c}_{\breve{s}}^T(\mathbf{x},\mathbf{y})\mathbf{\Sigma}^{-1}\mathbf{y}(t)$. Upon denoting the M_r-vector that collects the $(\sum_{r'=1}^{r-1} M_{r'}+1)$th to the $(\sum_{r'=1}^{r} M_{r'})$th entries of $\mathbf{c}_{\breve{s}}^T(\mathbf{x},\mathbf{y})\mathbf{\Sigma}^{-1}$ as $\boldsymbol{\sigma}_r^T$, a distributed algorithm can be devised in the same manner used to derive (17) and (18), i.e., obtain $\xi(t)$ per node through (17) and (18), with $\boldsymbol{\chi}_r^{(j)}(t)$ and $\mathbf{H}_r$ replaced by $\xi_r^{(j)}(t)$ and $\boldsymbol{\sigma}_r^T$, respectively.

IV. Application to Cognitive Radio Resource Allocation

In this section, the usefulness of the CG map information is demonstrated in the context of CR networks. The CRs aim at making opportunistic use of the spectrum by identifying unused spectral resources or *spectrum holes* in the frequency, time, and space domains [19]. The key enablers for CR operation include sensing and resource allocation.

Once the information on the activities of the licensed primary users (PUs) is acquired through sensing, the CR network can perform resource allocation to make the most use of the available transmission opportunities. Here, it is assumed that power control is employed to restrict the interference exposed to the PU links. For simplicity, suppose that a single-PU transmitter has been detected to be active at location $\mathbf{x}_s$ at transmit-power level p_s. The exposition can easily be extended to the multi-PU case. The positions of the PU *receivers* are assumed unknown.

To maximize its own transmission rate, the CR transmitter needs to maximize the transmit power while adhering to the interference constraints. The global CG map can provide valuable information in this setup, allowing us to predict the potential locations of the PU receivers, as well as the maximum interference-free transmit power (MIFTP) [13] that the CR transmitter can afford.

Let $\Pi(\mathbf{x})$ denote the power (in decibels) that is received at location $\mathbf{x} \in \mathcal{A}$ due to the PU transmission, which can be expressed as $\Pi(\mathbf{x}) = P_s + G_0 - 10\gamma\log_{10}\|\mathbf{x}_s - \mathbf{x}\| + s_{\mathbf{x}_s\to\mathbf{x}}$, where $P_s \triangleq 10\log_{10} p_s$, and the time index t has been suppressed for brevity. Based on the estimated CG map, $\Pi(\mathbf{x})$ can be modeled as Gaussian with mean $P_s + G_0 - 10\gamma\log_{10}\|\mathbf{x}_s - \mathbf{x}\| + \hat{s}_{\mathbf{x}_s\to\mathbf{x}}$ and variance $\sigma^2_{s_{\mathbf{x}_s\to\mathbf{x}}}$, which is given by (13), with $\mathbf{x}$ and $\mathbf{y}$ replaced by $\mathbf{x}_s$ and $\mathbf{x}$, respectively.

Because a PU receiver can reliably decode the desired message only if the received power level exceeds a threshold $\Pi_{\min}$ (in decibels), we can compute the probability of coverage that a PU receiver at location $\mathbf{x}$ would experience as

$$P_{\text{cov}}(\mathbf{x}) \triangleq \Pr\{\Pi(\mathbf{x}) \geq \Pi_{\min}\} = Q\left(\frac{\Pi_{\min} - P_s - G_0 + 10\gamma\log_{10}\|\mathbf{x}_s - \mathbf{x}\| - \hat{s}_{\mathbf{x}_s\to\mathbf{x}}}{\sigma_{s_{\mathbf{x}_s\to\mathbf{x}}}}\right) \tag{20}$$

where $Q(\cdot)$ is the standard Gaussian tail function. Then, the PU coverage region can be defined as the set of locations in $\mathcal{A}$, for which the coverage probability is no smaller than a threshold ν_s, i.e., $\mathcal{C}_s \triangleq \{\mathbf{x} \in \mathcal{A} | P_{\text{cov}}(\mathbf{x}) \geq \nu_s\}$. Note that, in the absence of CG map knowledge, we need to set $\hat{s}_{\mathbf{x}_s\to\mathbf{x}} = 0$. Then, $\mathcal{C}_s$ will reduce to a time-invariant disc that is centered at $\mathbf{x}_s$. The CG map estimate provides an invaluable means to overcome this oversimplification and more accurately portray the coverage region.

To obtain the MIFTP for CR transmission, the power that is received at position $\mathbf{x}$ due to a CR transmitter that is located at $\mathbf{x}_r$ and employs transmit power P_r (in decibels) can similarly be characterized as a Gaussian random variable with mean $P_r + G_0 - 10\gamma\log_{10}\|\mathbf{x}_r - \mathbf{x}\|_2 + \hat{s}_{\mathbf{x}_r\to\mathbf{x}}$ and variance $\sigma^2_{s_{\mathbf{x}_r\to\mathbf{x}}}$. Thus, the probability that the CR interference at position $\mathbf{x}$ exceeds a prescribed threshold $I_{\max}$ is given by

$$P_{\text{int}}(\mathbf{x}) = Q\left(\frac{I_{\max} - P_r - G_0 + 10\gamma\log_{10}\|\mathbf{x}_r - \mathbf{x}\|_2 - \hat{s}_{\mathbf{x}_r\to\mathbf{x}}}{\sigma_{s_{\mathbf{x}_r\to\mathbf{x}}}}\right). \tag{21}$$

The MIFTP can then be defined as the maximum value of P_r that yields a $P_{\text{int}}(\mathbf{x})$ no larger than a given outage threshold $\nu_r > 0$ for all

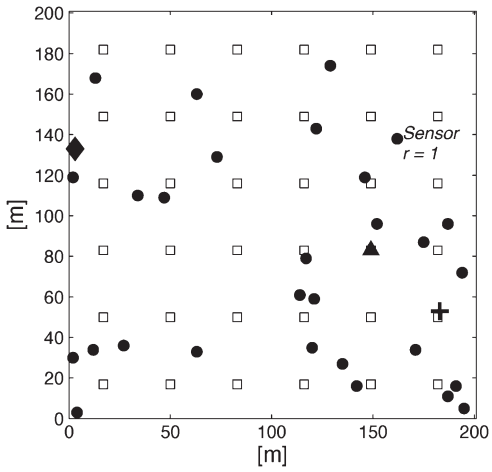

Fig. 1. Simulation setup.

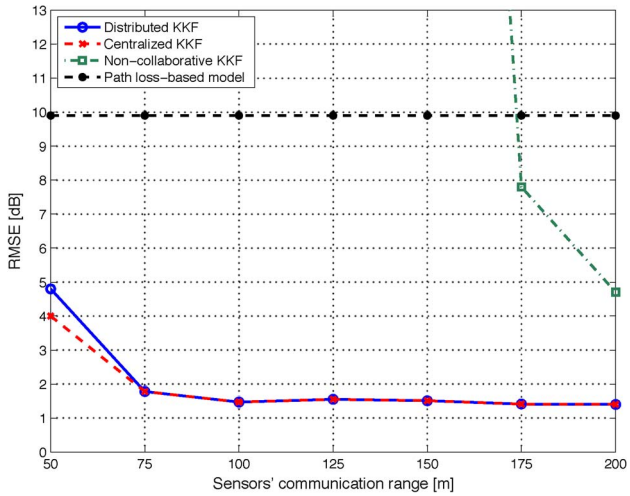

Fig. 2. Map estimation RMSEs.

potential receivers in the PU coverage region, i.e.,

$$P_r^* \triangleq \max P_r \quad \text{subject to} \quad P_{\text{int}}(\mathbf{x}) \leq \nu_r \qquad \forall\, \mathbf{x} \in \mathcal{C}_s. \tag{22}$$

With $\hat{s}_{\mathbf{x}_r \to \mathbf{x}}$ and $\sigma_{s_{\mathbf{x}_r \to \mathbf{x}}}$ available from the CG map estimators in the previous section, it is clearly possible to find P_r^* numerically.

V. Numerical Tests

Numerical tests were performed to verify the proposed algorithms. A 200 m $\times$ 200 m area was considered, and $N_r = 30$ CRs were deployed at the locations marked by circles in Fig. 1. The path-loss parameters were set to $G_0 = 0$ dB and $\gamma = 3$. The measurement noise $\epsilon_{\mathbf{x}_j \to \mathbf{x}_r}(t)$ had variance 10 throughout. For basis expansion, $K = 15$ Legendre polynomials were used.

The shadow fading was generated through the model in Section II, with $w(\mathbf{x}, \mathbf{u}) = w_0 \exp(\|\mathbf{x} - \mathbf{u}\|/d_w)$, where $w_0 = 7.3 \times 10^{-3}$ and $d_w = 50$ m were used, and the covariance of $\eta(\mathbf{x}, t)$ was set to $\mathbb{E}\{\eta(\mathbf{x}_1, t)\eta(\mathbf{x}_2, \tau)\} = \sigma_\eta^2 \exp(\|\mathbf{x}_1 - \mathbf{x}_2\|/d_\eta)\delta(t - \tau)$, with $\sigma_\eta = 0.25$ and $d_\eta = 30$ m. The model parameters for $\tilde{\ell}(\mathbf{x}, t)$ were set to $\sigma_{\tilde{s}} = 0.5$ dB and $d_{\tilde{\ell}} = 30$ m. The shadow fading generated had a mean of 0 dB and a standard deviation of 10 dB. The parameters of the state-space model were estimated from the generated shadowing, as discussed in Section III-B.

To assess the map-tracking performance of the proposed algorithm, the CG estimation errors were averaged over the 35 links from each of the uniformly spread grid points, which are denoted by the squares in Fig. 1, to position (149,83), marked with a black triangle in the same figure, as well as over 20 independent shadowing realizations. It was assumed that two sensors could communicate only if they were within a given communication range d_{comm}, i.e., $\mathcal{M}_r = \{j | j \neq r, \|\mathbf{x}_r - \mathbf{x}_j\| \leq d_{\text{comm}}\}$. Thus, d_{comm} essentially limits the number of CG measurements that each sensor can obtain. Fig. 2 depicts the root mean square errors (RMSEs) of i) the DKKF algorithm proposed in this paper; ii) its centralized counterpart; iii) the non-collaborative KKF at CR $r = 1$ (see Fig. 1), in which the sensor uses only its local CG measurements; and iv) the path loss-only map. The value of d_{comm} was varied in [50, 200] m, and the number of sensors was $N_r = 30$. For DKKF, 100 consensus iterations were performed per time t, and $\{\mathcal{N}_r\}$ are assumed to coincide with sets $\{\mathcal{M}_r\}$.

Fig. 2 shows that the proposed collaborative algorithm clearly outperforms the non-collaborative alternative. This case happens because the noncollaborative algorithm uses only M_1 local CG measurements, whereas the collaborative KKF makes use of all M measurements through consensus iterations. Certainly, it would be challenging for the noncollaborative algorithm to predict the shadow fading for a transmitter that is far from CR 1 due to the lack of informative measurements, whereas the collaborative algorithm can extract a single coherent view of the global shadowing field. As d_{comm} increases, the noncollaborative approach performs considerably better due to the increased number of measurements but still remains inferior to the collaborative approach. Note that, when d_{comm} is very small, the performance of the distributed algorithm slightly degrades compared to the centralized algorithm, because a larger number of hops would be necessary to achieve full consensus.

Next, to illustrate the merits of the global CG map in the CR context, the resource allocation problem is considered. A network of $N_r = 20$ CRs with $d_{\text{comm}} = 125$ m was used. Given an active PU that transmits at $P_s = 0$ dBW from location $\mathbf{x}_s = (3, 133)$, which is marked by the diamond marker in Fig. 1, a realization of the true received power map $\Pi(\mathbf{x})$ due to the PU transmission is depicted using the contour plot in Fig. 3(a). Superimposed in Fig. 3(a) is another contour plot of the true CG map $G_{\mathbf{x}_r \to \mathbf{x}}$ from a CR transmitter at $\mathbf{x}_r = (183, 53)$ and marked by a "+" in Fig. 1. Note that the contours are not concentric circles due to the shadowing effect. Thus, estimating the shadowing field is essential for efficient CR resource allocation. An estimated version of Fig. 3(a) using DKKF is shown in Fig. 3(b). Based on the estimated CG map, the PU coverage region was estimated for $\Pi_{\min} = -60$ dBW and $\nu_s = 0.4$, which is depicted by round dots in Fig. 4(a). Setting $\nu_s < 0.5$ yields a conservative characterization of the PU coverage region, as can be confirmed by noting that the -60-dBW contour of the received power map in Fig. 3(a) is contained by the estimated PU coverage region in Fig. 4(a). The MIFTP for the CR transmitter with $I_{\max} = -40$ dBm and $\nu_r = 0.01$ was found to be 28.9 dBm. The estimated region in which the interference power due to the CR transmission is no less than $I_{\max}$ with probability at least ν_r is shown with square dots in Fig. 4(a). Note that, although the estimated MIFTP is quite conservative compared with the true MIFTP of 35.5 dBm, it is vastly improved compared with the path-loss-only map-based calculation, which yields an MIFTP of only -10.5 dBm. The PU coverage region, as well as the interference region based on the path-loss map, is shown in Fig. 4(b). It is shown that the PU coverage region is grossly overestimated.

VI. Conclusion

An algorithm that can track the spatiotemporal evolution of the RF channels in a given geographical area has been developed. Adopting a dynamic shadowing model, which can capture both spatial and

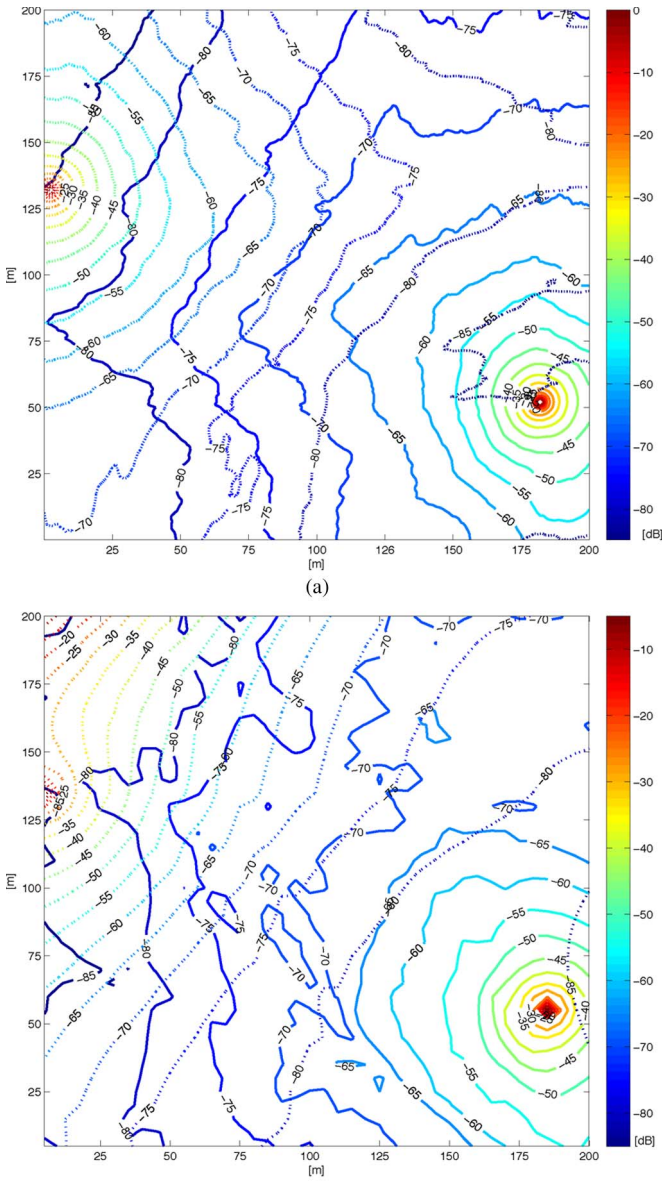

Fig. 3. RF power map due to PU transmission and CG map for a CR transmitter. (a) True. (b) Estimated.

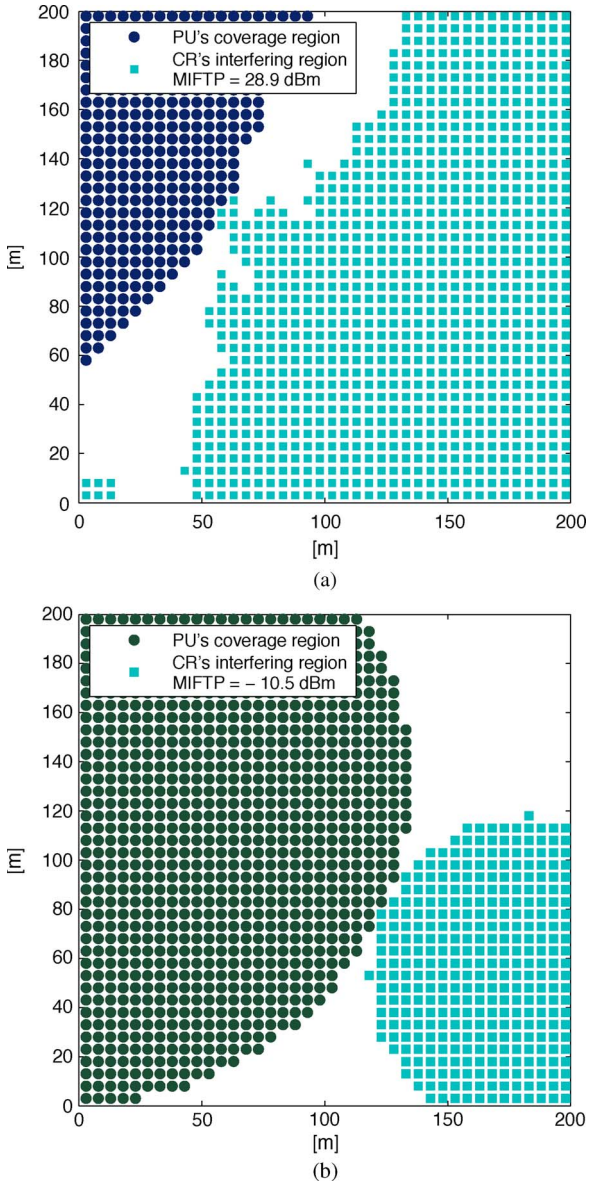

Fig. 4. Estimated PU coverage and CR interference regions. (a) KKF based. (b) Path loss based.

temporal correlations, the novel KKF-based algorithm was shown to obtain MMSE-optimal estimates of unknown CGs of wireless links at arbitrary transceiver locations in the area, using measurements taken by a network of CRs. A distributed version of the KKF algorithm, which requires only local message passing, was derived using the ADMoM framework. The proposed collaborative map tracking algorithm showed excellent performance, especially when compared with the non-collaborative counterpart in terms of map mean square error (MSE). In addition, the merits of the proposed algorithm were highlighted in challenging CR scenarios.

References

[1] Y. Zhao, L. Morales, J. Gaeddert, K. K. Bae, J.-S. Um, and J. H. Reed, "Applying radio environment maps to cognitive wireless regional area networks," in *Proc. DySPAN Conf.*, Dublin, Ireland, Apr. 2007, pp. 115–118.

[2] M. Gudmundson, "Correlation model for shadow fading in mobile radio systems," *Electron. Lett.*, vol. 27, no. 23, pp. 2145–2146, Nov. 1991.

[3] Z. Wang, E. K. Tameh, and A. Nix, "Simulating correlated shadowing in mobile multihop relay/ad hoc networks," Univ. Bristol, Bristol, U.K., IEEE C802.16j-06/060, Jul. 2006.

[4] C. Oestges, N. Czink, B. Bandemer, P. Castiglione, F. Kaltenberger, and A. J. Paulraj, "Experimental characterization and modeling of outdoor-to-indoor and indoor-to-indoor distributed channels," *IEEE Trans. Veh. Technol.*, vol. 59, no. 5, pp. 2253–2265, Jun. 2010.

[5] P. Agrawal and N. Patwari, "Correlated link shadow fading in multi-hop wireless networks," *IEEE Trans. Wireless Commun.*, vol. 8, no. 9, pp. 4024–4036, Aug. 2009.

[6] J. Riihijärvi, P. Mähönen, M. Wellens, and M. Gordziel, "Characterization and modelling of spectrum for dynamic spectrum access with spatial statistics and random fields," in *Proc. PIMRC Conf.*, Cannes, France, Sep. 2008, pp. 1–6.

[7] S. Barbarossa, G. Scutari, and T. Battisti, "Cooperative sensing for cognitive radio using decentralized projection algorithms," in *Proc. SPAWC Conf.*, Perugia, Italy, Jun. 2009, pp. 116–120.

[8] J.-A. Bazerque and G. B. Giannakis, "Distributed spectrum sensing for cognitive radio networks by exploiting sparsity," *IEEE Trans. Signal. Process.*, vol. 58, no. 3, pp. 1847–1862, Mar. 2010.

[9] G. Mateos, J.-A. Bazerque, and G. B. Giannakis, "Spline-based spectrum cartography for cognitive radios," in *Proc. 43rd Asilomar Conf. Signals, Syst., Comput.*, Pacific Grove, CA, Nov. 2009.

[10] S.-J. Kim, E. Dall'Anese, and G. Giannakis, "Cooperative spectrum sensing for cognitive radios using kriged Kalman filtering." *IEEE J. Sel. Topics Signal Process.*, vol. 5, no.1, pp. 24–36, Feb. 2011.
[11] K. S. Butterworth, K. W. Sowerby, and A. G. Williamson, "Base station placement for in-building mobile communication systems to yield high capacity and efficiency," *IEEE Trans. Commun.*, vol. 48, no. 4, pp. 658–669, Apr. 2000.
[12] K. Kumaran, S. E. Golowich, and S. Borst, "Correlated shadow-fading in wireless networks and its effect on call dropping," *Wirel. Netw.*, vol. 8, no. 1, pp. 61–71, Jan. 2002.
[13] B. Mark and A. Nasif, "Estimation of maximum interference-free power level for opportunistic spectrum access," *IEEE Trans. Wireless Commun.*, vol. 8, no. 5, pp. 2505–2513, May 2009.
[14] T. S. Rappaport, *Wireless Communications: Principles and Practice*. Upper Saddle River, NJ: Prentice-Hall, 1996.
[15] K. V. Mardia, C. Goodall, E. J. Redfern, and F. J. Alonso, "The kriged Kalman filter," *Test*, vol. 7, no. 2, pp. 217–285, Dec. 1998.
[16] C. K. Wikle and N. Cressie, "A dimension-reduced approach to space–time Kalman filtering," *Biometrika*, vol. 86, no. 4, pp. 815–829, Dec. 1999.
[17] J. Cortés, "Distributed kriged Kalman filter for spatial estimation," *IEEE Trans. Autom. Control*, vol. 54, no. 12, pp. 2816–2827, Dec. 2009.
[18] B. D. Ripley, *Spatial Statistics*. Hoboken, NJ: Wiley, 1981.
[19] X. Hong, C. Wang, H. Chen, and Y. Zhang, "Secondary spectrum access networks," *IEEE Veh. Technol. Mag.*, vol. 4, no. 2, pp. 36–43, Jun. 2009.

Selected Mapping Algorithm for PAPR Reduction of Space-Frequency Coded OFDM Systems Without Side Information

Mahmoud Ferdosizadeh Naeiny and
Farokh Marvasti, *Senior Member, IEEE*

***Abstract*—Selected mapping (SLM) is a well-known technique for peak-to-average-power ratio (PAPR) reduction of orthogonal frequency-division multiplexing (OFDM) systems. In this technique, different representations of OFDM symbols are generated by rotation of the original OFDM frame by different phase sequences, and the signal with minimum PAPR is selected and transmitted. To compensate for the effect of the phase rotation at the receiver, it is necessary to transmit the index of the selected phase sequence as side information (SI). In this paper, an SLM technique is introduced for the PAPR reduction of space-frequency-block-coded OFDM systems with Alamouti coding scheme. Additionally, a suboptimum detection method that does not need SI is introduced at the receiver side. Simulation results show that the proposed SLM method effectively reduces the PAPR, and the detection method has performance very close to the case where the correct index of the phase sequence is available at the receiver side.**

***Index Terms*—Orthogonal frequency-division multiplexing (OFDM), peak-to-average-power ratio (PAPR), selected mapping (SLM), space frequency block coded (SFBC), spatial diversity.**

Manuscript received May 26, 2010; revised September 19, 2010 and November 21, 2010; accepted January 3, 2011. Date of publication January 28, 2011; date of current version March 21, 2011. The review of this paper was coordinated by Prof. R. Schober.

The authors are with the Advanced Communication Research Institute and the Department of Electrical Engineering, Sharif University of Technology, Tehran 11365-9363, Iran (e-mail: mferdosi@ee.sharif.edu; marvasti@sharif.edu).

Color versions of one or more of the figures in this paper are available online at http://ieeexplore.ieee.org.
Digital Object Identifier 10.1109/TVT.2011.2109070

I. Introduction

Orthogonal frequency-division multiplexing (OFDM) is a well-known technique for transmission of high rate data over broadband frequency-selective channels [1]. One of the drawbacks of OFDM systems is high peak-to-average-power ratio (PAPR), which leads to the saturation of the high-power amplifier. Thus, a high-dynamic-range amplifier is needed, which increases the cost of the system. The frequency-domain symbols of an OFDM frame is denoted by $\mathbf{X} = [X(0), X(1), \ldots, X(N_c - 1)]^T$, where N_c is the number of subcarriers. It is assumed that $X(k) \in \mathcal{C}$, where $\mathcal{C}$ is the set of constellation points. The vector $\mathbf{x} = [x(0), x(1), \ldots, x(N-1)]^T$ contains the time-domain samples of the complex baseband OFDM signal as given by

$$x(n) = \frac{1}{\sqrt{N}} \sum_{k=0}^{N_c - 1} X(k) e^{j\frac{2\pi nk}{N}} \tag{1}$$

where $j = \sqrt{-1}$, and N/N_c is the oversampling ratio. It is clear that $\mathbf{x} = \text{IFFT}_N\{\mathbf{X}\}$, where $\text{IFFT}_N\{\}$ is the N-point inverse fast Fourier transform (IFFT) operation. The PAPR of the OFDM frame is defined by

$$\text{PAPR}(\mathbf{x}) = \frac{\max_n \left\{|x(n)|^2\right\}}{E\left\{|x(n)|^2\right\}} \tag{2}$$

where $E\{.\}$ is the mathematical expectation. According to (1), the time-domain samples are the sum of N_c independent terms. When N_c is large, based on the central limit theorem, the time-domain samples have a Gaussian distribution; thus, they may have large amplitudes [2]. To overcome this problem, some algorithms have been proposed, which reduce the PAPR of the baseband OFDM signal [3]–[16]. Some of these methods need side information (SI) to be transmitted to the receiver, such as partial transmit sequence [3], [4] and selected mapping (SLM) [5]–[7]. Some other methods do not need SI, such as clipping and filtering [8], [9], tone reservation [10], [11], block coding [12], [13], and active constellation extension [14].

In the SLM method, D different representations of the OFDM frame are generated, and that with minimum PAPR is transmitted. If the vectors $[\phi^d(0), \phi^d(1), \ldots, \phi^d(N_c - 1)]^T, d = 0, 1, \ldots, D-1$, are D random phase sequences with the length of N_c and $\mathbf{b}^d = [e^{j\phi^d(0)}, e^{j\phi^d(1)}, \ldots, e^{j\phi^d(N_c-1)}]^T$, then D representations of the signal $\mathbf{x}$ are

$$\mathbf{x}^d = \text{IFFT}_N\{\mathbf{X} \otimes \mathbf{b}^d\}, \qquad 0 \le d \le D-1 \tag{3}$$

where $\otimes$ is element-by-element production. The index of the optimum phase sequence is

$$\bar{d} = \underset{d \in \{0,1,\ldots,D-1\}}{\arg\min} \left\{\text{PAPR}\{\mathbf{x}^d\}\right\}. \tag{4}$$

To reduce the complexity of the application of different phase sequences, often, phases $\phi^d(k)$ are randomly chosen from $\{0, \pi\}$. This means that $b^d(k) \in \{\pm 1\}$, and it is enough to change the sign of the symbols $X(k)$ before IFFT operation. The signal $\mathbf{x}^{\bar{d}}$ is transmitted, and the index of selected phase sequence $\bar{d}$ is sent to the receiver as SI. If the SI is received with an error, the OFDM frame will be lost; thus, this information must be protected by coding. Several SLM methods have been proposed for single-antenna OFDM systems, which do not need explicit SI [15]–[17]. Some of these algorithms pay a penalty for the transmission power [15], [16]. The drawback of the method introduced in [17] is that the phase sequences must be chosen such